STRUCTURE OF A FLOW OVER A ROTATING DISK

Mbolahasina S. RALIJAONA[1], Sahoby LALAOHARISOA[2], Tsilavo M. RAZAFINDRAZAKA[3], Adolphe A. RATIARISON[4]

[1] *PhD student, Atmosphere, Climate and Oceans Dynamics Laboratory (DyACO), Physics and Applications, Sciences and Technologies Domain, University of Antananarivo, Madagascar*
[2] *PhD student, Atmosphere, Climate and Oceans Dynamics Laboratory (DyACO), Physics and Applications, Sciences and Technologies Domain, University of Antananarivo, Madagascar*
[3] *Maître de Conférences, Institut Supérieur de Technologie d'Antananarivo, Madagascar*
[4] *Professeur Titulaire, Atmosphere, Climate and Oceans Dynamics Laboratory (DyACO), Physics and Applications, Sciences and Technologies Domain, University of Antananarivo, Madagascar*

ABSTRACT

The structure of a rotating flow is studied by Reynolds-averaged Navier-Stokes (RANS) numerical simulation. The fluid is contained in a cylindrical tank with fixed vertical sidewall. The flow is driven by the rotation of the bottom plate. The free surface shape is calculated by the level set method, and this study is restricted to the case where the free surface is plane. During simulations, the fluid taken into account is water. The Reynolds number and the aspect ratio of the flow are the varying parameters. The values of The Reynolds number used in the simulations are 10^4, 10^5, *and* 10^6, *for the aspect ratio, they are 0.66, 1 and 1.33. Velocity fields variations are represented along three different radial line segments. One at the bottom of the cylinder, one at the half of the initial fluid height, and the last at the free surface. The velocity magnitude increases with time and when Reynolds number grows. Radial and azimuthal velocity components decrease with growing aspect ratio, and vertical velocity keeps the same scale. For every value of the parameters, the motion direction is described as followed: at the rotating bottom, the fluid goes from the center to the sidewall, near which it is upward. At the free surface and at half of its height, the fluid is tending to move toward the center. And at a certain distance from the fixed sidewall, the fluid motion is downward. This flow structure is consistent with the structure found in experimental studies reported in [5] and [6].*

Keyword: - *rotating flow, Reynolds-averaged Navier-Stokes (RANS), free surface, level set method.*

1. INTRODUCTION

Rotating flows are subject of research because of their applications in geophysical fluids and in engineering domain. In particular, flow over rotating disks have been highly investigated in the past two decades. The most popular configuration used consist of a cylindrical tank with rotating bottom and fixed sidewall, filled with a liquid. This particular interest comes from the fact that its free surface is the seat of a phenomenon called the rotating polygons in the literature [1,2,3,4,5,6,7,8]. This phenomenon appears by the loss of axial symmetry and the formation of polygonal patterns on the free surface [5,6]. When the rotation rate of the bottom is high enough, the free surface shows polygonal patterns [6]. Polygons with up to 8 corners have been observed in [9] as shown in ***fig -1***.

The structure of this type of flow was described in [5] and [6] as having an azimuthal flow in the same direction as the rotating bottom, outward at the rotating bottom, inward at the free surface and upward near the fixed cylinder wall. The goal of this work is to determine if the structure of the flow with a numerical model shows the same characteristics than in these experimental cases. The numerical model adopted is the Reynolds-averaged Navier-Stokes equations (RANS) implemented with the finite element method.

In this paper, section 2 is devoted to the governing equations. The RANS equations are used for simulating the fluid flow, and the level set method for calculating the free surface shape. The results are in section 3, where the motion of the fluid in the radial, azimuthal and vertical directions are presented. Then conclusion is in section 4.

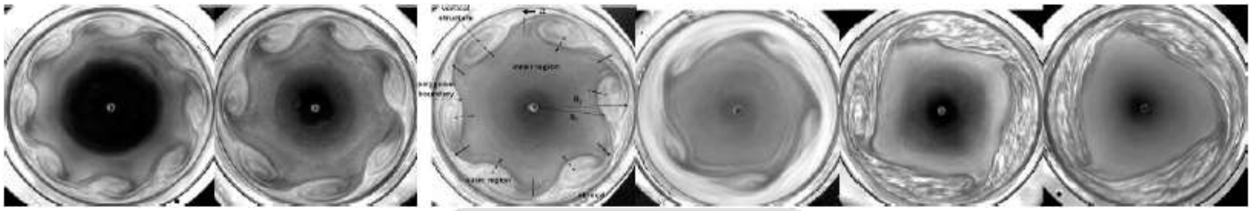

Fig -1: Polygons on free surface from 8 to 3 corners (source [9])

2. GOVERNING EQUATIONS

The cylindrical container in which the fluid is in motion is sketched ***fig -2***. In this work, the fluid used in simulations is water. Velocity and pressure prevailing within the flow are obtained by solving the Navier-Stokes equations, and the free surface shape is determined by the level set method.

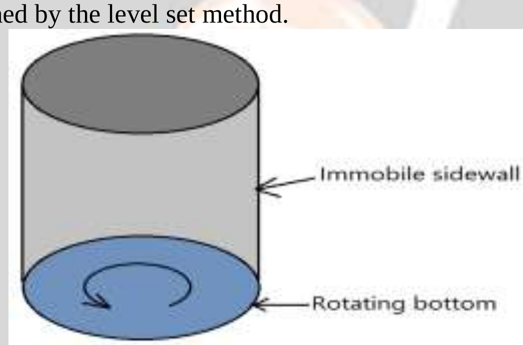

Fig -2: Cylindrical tank

2.1 Turbulence Modelling

Newtonian fluids flow is governed by the Navier-Stokes equations:

$$\frac{\partial \vec{u}}{\partial t} + \left(\vec{u}.\vec{\nabla}\right)\vec{u} - \nu \Delta \vec{u} + \frac{\vec{\nabla} p}{\rho} = \frac{\vec{f}}{\rho} \tag{1.1}$$

Solving the Navier-Stokes equations for turbulent flows is highly expensive in terms of time and memory. To avoid these constraints, the Reynolds Averaged Navier-Stokes (RANS) equations are solved instead of the the Navier-Stokes equations. RANS equations are obtained by decomposing velocity and pressure in mean and fluctuating part:

$$u_i = \overline{u}_i + u_i', \; p = \overline{p} + p' \tag{1.2}$$

where u_i is the i^{th} component of the velocity.

Substituting equation (1.2) in equation (1.1) leads to the appearance of the Reynolds-stress term $\tau_{ij} = \overline{u_i' u_j'}$ which contains six new unknowns. There are several methods to obtain those new unknowns, leading to different models. The one used in this work is the called K-ω model. As mentioned in [10], the system of partial differential equations of the K-ω model is:

$$\frac{\partial \overline{u}_i}{\partial t} + \overline{u}_j \frac{\partial \overline{u}_i}{\partial x_j} = -\frac{\partial \overline{p}}{\partial x_i} + \nu \frac{\partial^2 \overline{u}_i}{\partial x_j \partial x_j} - \frac{\partial \tau_{ij}}{\partial x_j} \tag{1.3}$$

$$\frac{\partial \overline{u}_i}{\partial x_i} = 0 \tag{1.4}$$

$$\frac{\partial K}{\partial t} + \overline{u}_i \frac{\partial K}{\partial x_i} = -\tau_{ij} \frac{\partial \overline{u}_i}{\partial x_j} - C^* \frac{K^{3/2}}{l_0} + \frac{\partial}{\partial x_i}\left(\frac{\nu_T}{\sigma_K} \frac{\partial K}{\partial x_i} \right) + \nu \frac{\partial^2 K}{\partial x_i \partial x_i} \tag{1.5}$$

$$\tau_{ij} = \frac{2}{3} K \delta_{ij} - \nu_T \left(\frac{\partial \overline{u}_i}{\partial x_j} + \frac{\partial \overline{u}_j}{\partial x_i} \right) \tag{1.6}$$

$$\frac{\partial \omega}{\partial t} + \overline{u}_i \frac{\partial \omega}{\partial x_i} = -\gamma_1 \frac{\omega}{K} \tau_{ij} \frac{\partial \overline{u}_i}{\partial x_j} + \frac{\partial}{\partial x_i}\left(\frac{\nu_T}{\sigma_\omega} \frac{\partial \omega}{\partial x_i} \right) - \gamma_2 \omega^2 + \nu \frac{\partial^2 \omega}{\partial x_i \partial x_i} \tag{1.7}$$

$$\nu_T = \gamma^* \frac{K}{\omega} \tag{1.8}$$

where Einstein summation convention is applied when indices is repeated, $K = \frac{1}{2}\overline{u_i ' u_i '}$ is the turbulent kinetic energy, γ_1, γ_2, γ^*, σ_ω, C^* and σ_K are nondimensional constants, l_0 is the turbulence length scale, $\omega = \frac{\varepsilon}{K}$ is the reciprocal turbulent time scale and ε is the turbulent dissipation rate.

2.2 Interface tracking

The free surface shape is calculated with the level set method. This method was first introduced by Osher and Sethian [11] and consist to introduce a level set function whose null value corresponds to the interface. Let Ω_1 be the domain containing the water, Ω_2 be the one containing the air and Γ_3 is their common boundary (the free surface). The level set function is defined as:

$$\varphi(x,y,z,t) > 0 \text{ for } M(x,y,z) \in \Omega_1$$
$$\varphi(x,y,z,t) < 0 \text{ for } M(x,y,z) \in \Omega_2$$
$$\varphi(x,y,z,t) = 0 \text{ for } M(x,y,z) \in \Gamma_3$$

The motion of the free surface is given by the convection of the level set function φ:

$$\frac{\partial \varphi}{\partial t} + \vec{u} \cdot \vec{\nabla} \varphi = 0 \tag{1.9}$$

where $\vec{u}$ is the velocity of the water.

3. FLOW STRUCTURE

The flow structure has been investigated for varying Reynolds number $\mathrm{Re} = R^2\Omega/\nu$ and aspect ratio $\Gamma = H/R$, where R is the radius of the cylindrical tank , Ω is the angular frequency of the rotating disk, ν is the kinematic viscosity of water and H is the initial free surface height and. Γ is varied by fixing the value of R and varying H . The range of Reynolds number used during simulations are 10^4, 10^5 and 10^6, and 0.66, 1 and 1.33 for the aspect ratio.

The velocity components are the cylindrical ones: radial, azimuthal and vertical components. The variation of each of these components are shown as a function of the radial coordinate r at three (3) different heights (at $z = 0$, at $z = H/2$ and at $z = H$). The variation of the velocity components according to time are also plotted. This work is restricted to the case where the flow has a flat free surface so the time duration along which the velocity is represented varies with the Reynolds number and the aspect ratio.

3.1 Flow in radial direction

The charts **Chart - *1*** to **Chart - *9*** shows that the radial velocity is positive at $z=0$ (left charts), and negative at the free surface and at the half of free surface height (respectively right charts and middle charts). The motion of the fluid is then centrifugal at the bottom of the tank and centripetal at $z=H/2$ and at $z=H$. The magnitude of u_r grows with the Reynolds number at the three different heights. When $\Gamma=0.66$ and at $z=0$ for example, the radial component is around $10^{-3}\ m.s^{-1}$ for $\mathrm{Re}=10^4$ (**Chart - *1*** left), around $10^{-2}\ m.s^{-1}$ for $\mathrm{Re}=10^5$ (**Chart - *2*** left), and around $10^{-1}\ m.s^{-1}$ for $\mathrm{Re}=10^6$ (**Chart - *3*** left). u_r decreases when Γ increases at the free surface: the maximum magnitude is $2.6\times10^{-4}\ m.s^{-1}$ when $\Gamma=0.66$ (**Chart - *1*** right), it decreases at $1.6\times10^{-4}\ m.s^{-1}$ when $\Gamma=1$ (**Chart - *4*** right), and at $1.5\times10^{-5}\ m.s^{-1}$ when $\Gamma=1.33$ (**Chart - *7*** right). The variation along the radial distance is as followed: u_r is first growing with the radial coordinate, then near the sidewall, it is decreasing. The radial component of the velocity is also increasing with time.

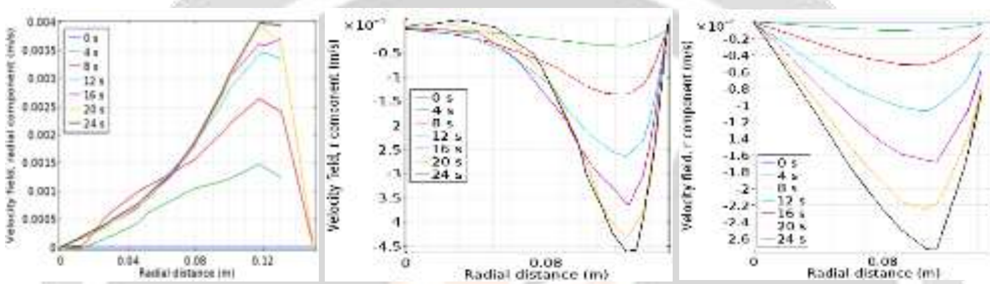

Chart - 1: Radial velocity when $\Gamma=0.66$ and $\mathrm{Re}=10^4$. Left: at $z=0$, middle: at $z=0.05$, right: at $z=0.1$.

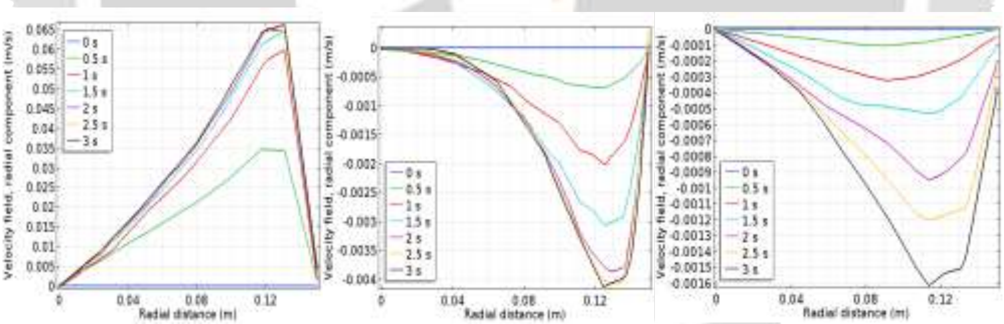

Chart - 2: Radial velocity when $\Gamma=0.66$ and $\mathrm{Re}=10^5$. Left: at $z=0$, middle: at $z=0.05$, right: at $z=0.1$.

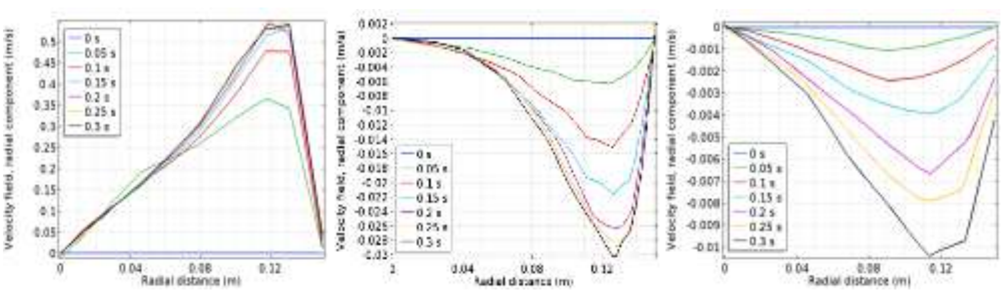

Chart - 3: Radial velocity when $\Gamma = 0.66$ and $\mathrm{Re} = 10^6$. Left: at $z = 0$, middle: at $z = 0.05$, right: at $z = 0.1$.

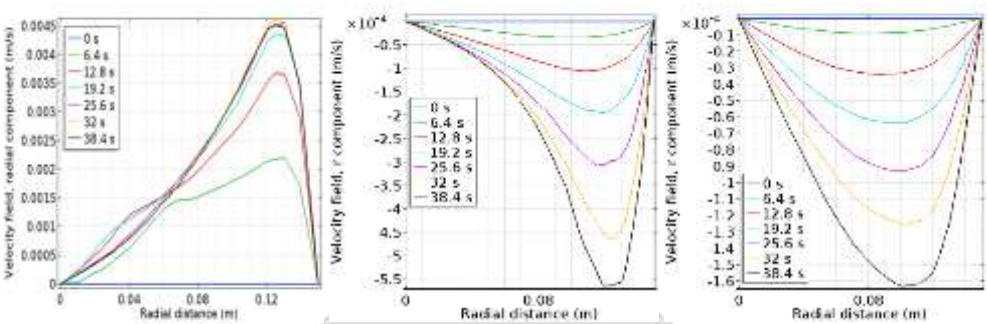

Chart - 4: Radial velocity when $\Gamma = 1$ and $\mathrm{Re} = 10^4$. Left: at $z = 0$, middle: at $z = 0.075$, right: at $z = 0.15$.

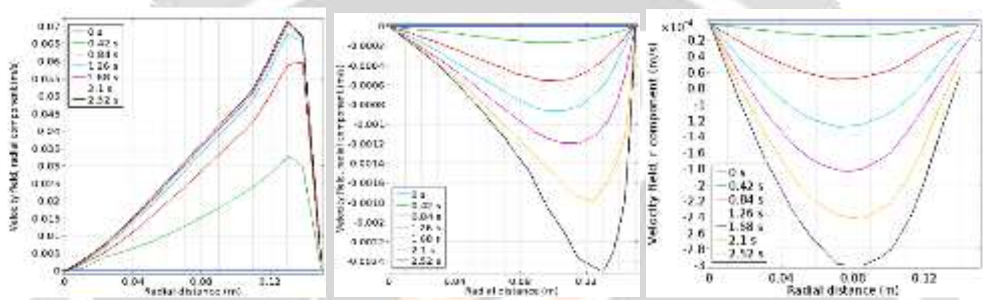

Chart - 5: Radial velocity when $\Gamma = 1$ and $\mathrm{Re} = 10^5$. Left: at $z = 0$, middle: at $z = 0.075$, right: at $z = 0.15$.

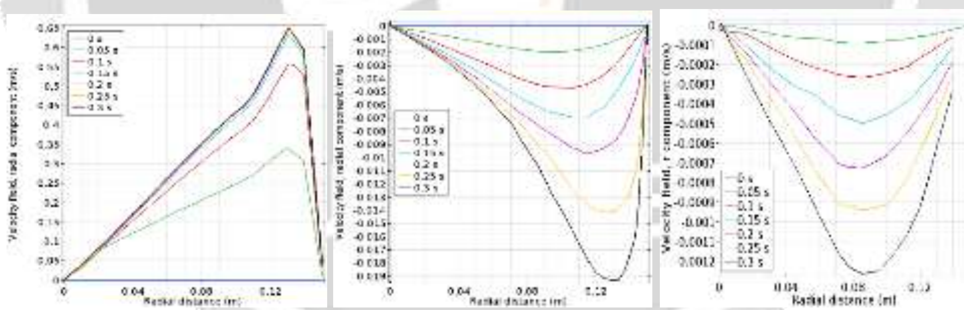

Chart - 6: Radial velocity when $\Gamma = 1$ and $\mathrm{Re} = 10^6$. Left: at $z = 0$, middle: at $z = 0.075$, right: at $z = 0.15$.

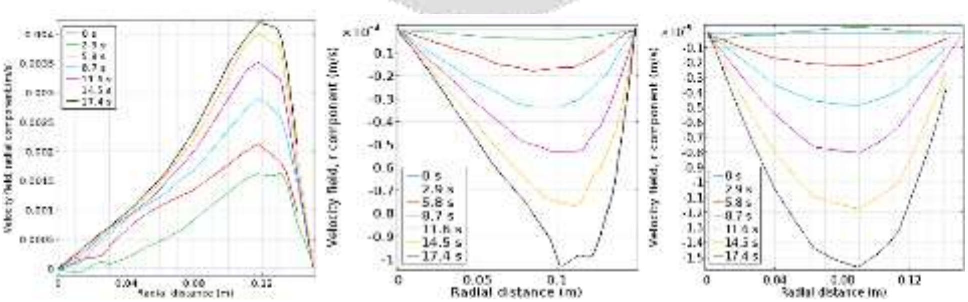

Chart - 7: Radial velocity when $\Gamma = 1.33$ and $\mathrm{Re} = 10^4$. Left: at $z = 0$, middle: at $z = 0.1$, right: at $z = 0.2$.

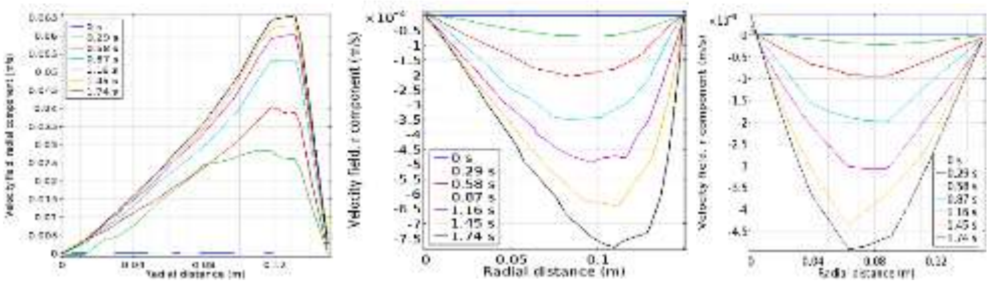

Chart - 8: Radial velocity when $\Gamma = 1.33$ and $\mathrm{Re} = 10^5$. Left: at $z = 0$, middle: at $z = 0.1$, right: at $z = 0.2$.

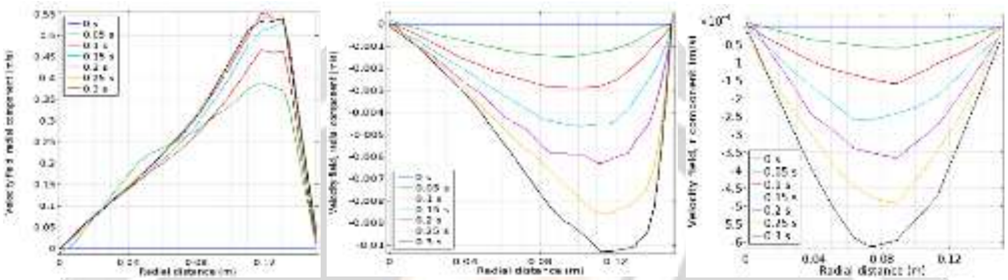

Chart - 9: Radial velocity when $\Gamma = 1.33$ and $\mathrm{Re} = 10^6$. Left: at $z = 0$, middle: at $z = 0.1$, right: at $z = 0.2$.

3.2 Flow in azimuthal direction

In this section, the characteristics of the azimuthal component of the velocity are presented. Its magnitude remains the same through time at the bottom of the container (**Chart - *10*** to **Chart - *18*** left), but increases with time at $z = H/2$ and at $z = H$ (**Chart - *10*** to **Chart - *18*** middle and right). The azimuthal velocity u_θ is decreasing with altitude, and consequently with the aspect ratio. On **Chart - *10*** for example, values of u_θ are around $10^{-2}\ m.s^{-1}$ at $z = 0$ (left chart), it decreases around $10^{-3}\ m.s^{-1}$ at $z = H/2$ (middle chart), and around $10^{-4}\ m.s^{-1}$ at the free surface (right chart). By comparing the values of the azimuthal velocity between the cases with same value of aspect ratio but with different Reynolds number, we can see that u_θ is increasing with increasing Reynolds number. Concerning its sign, it is generally positive. u_θ is negative in some case (**Chart - *16*** middle), but those negative value are close to zero and are due to the decreasing of the magnitude of u_θ with height. So, the fluid is turning in the same direction from bottom to free surface.

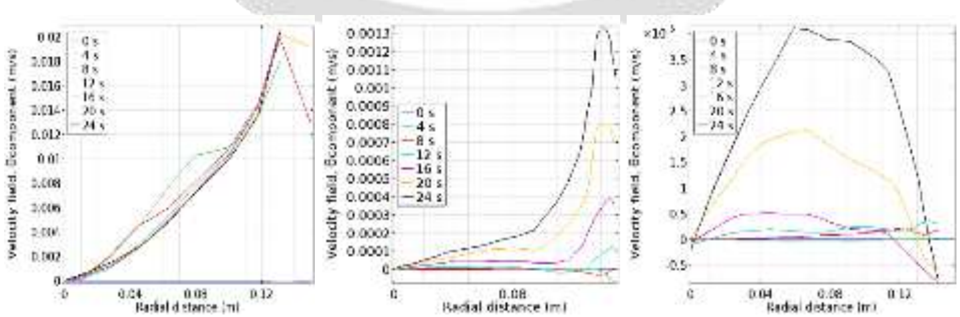

Chart - 10: Azimuthal velocity when $\Gamma = 0.66$ and $\mathrm{Re} = 10^4$. Left: at $z = 0$, middle: at $z = 0.05$, right: at $z = 0.1$.

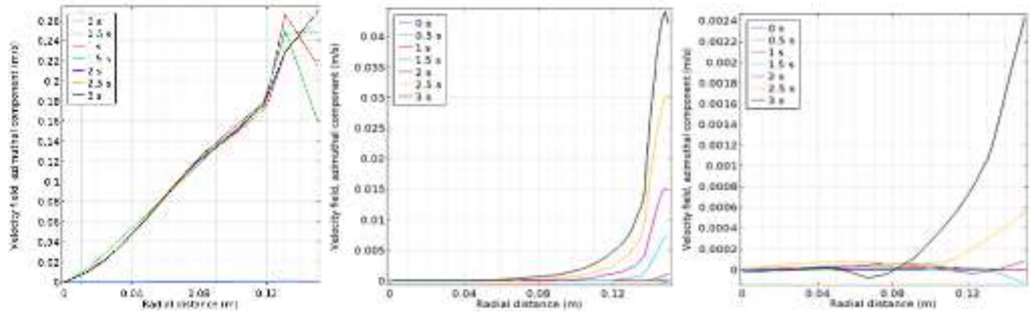

Chart - 11: Azimuthal velocity when $\Gamma = 0.66$ and $\mathrm{Re} = 10^5$. Left: at $z = 0$, middle: at $z = 0.05$, right: at $z = 0.1$.

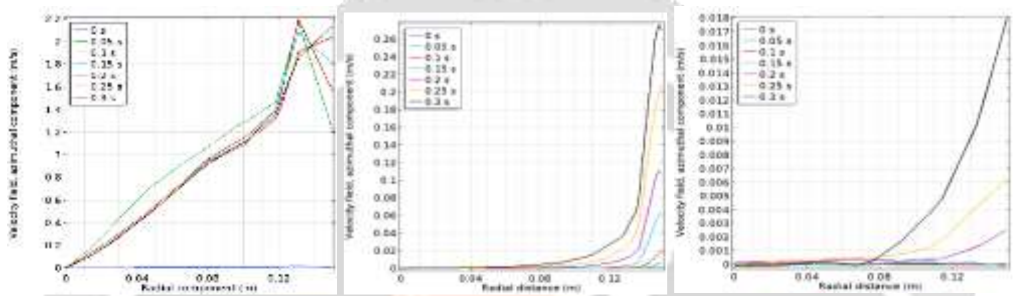

Chart - 12: Azimuthal velocity when $\Gamma = 0.66$ and $\mathrm{Re} = 10^6$. Left: at $z = 0$, middle: at $z = 0.05$, right: at $z = 0.1$.

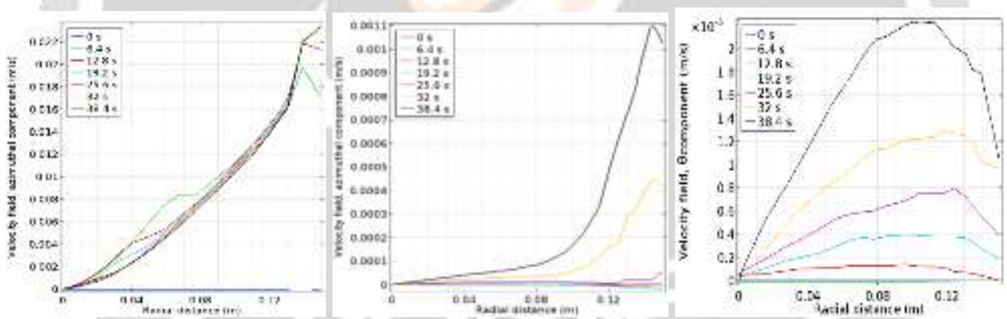

Chart - 13: Azimuthal velocity when $\Gamma = 1$ and $\mathrm{Re} = 10^4$. Left: at $z = 0$, middle: at $z = 0.075$, right: at $z = 0.15$.

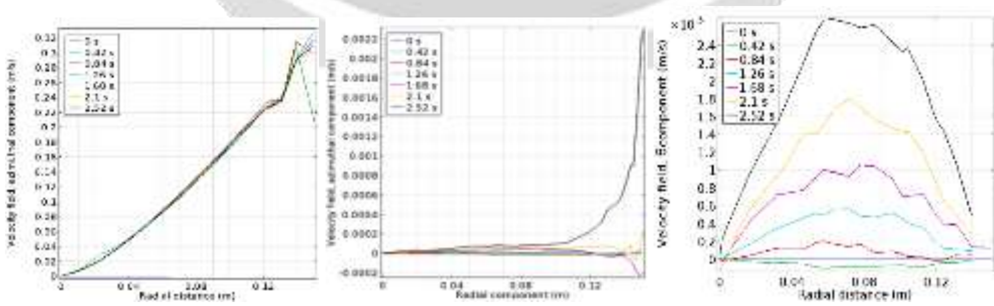

Chart - 14: Azimuthal velocity when $\Gamma = 1$ and $\mathrm{Re} = 10^5$. Left: at $z = 0$, middle: at $z = 0.075$, right: at $z = 0.15$.

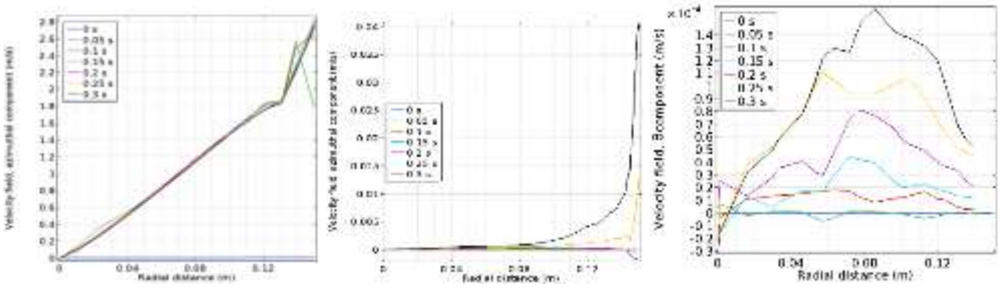

Chart - 15: Azimuthal velocity when $\Gamma = 1$ and $\mathrm{Re} = 10^6$. Left: at $z = 0$, middle: at $z = 0.075$, right: at $z = 0.15$.

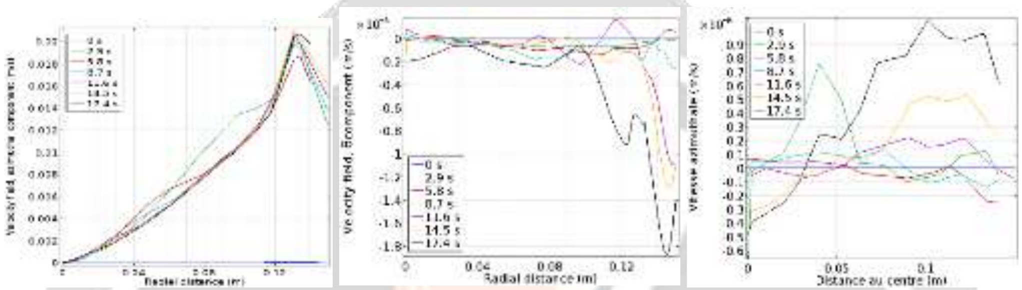

Chart - 16: Azimuthal velocity when $\Gamma = 1.33$ and $\mathrm{Re} = 10^4$. Left: at $z = 0$, middle: at $z = 0.1$, right: at $z = 0.2$.

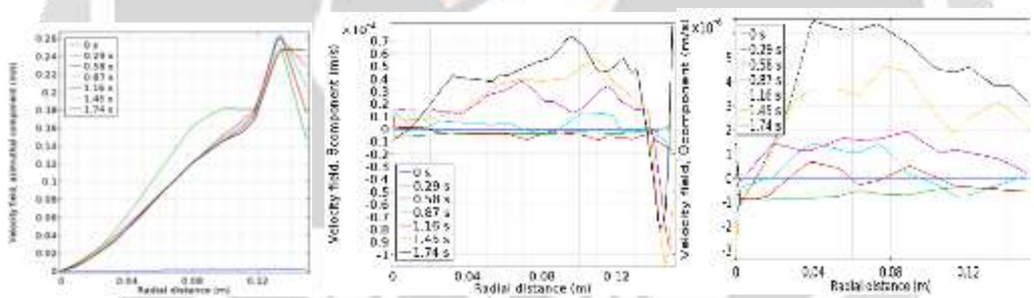

Chart - 17: Azimuthal velocity when $\Gamma = 1.33$ and $\mathrm{Re} = 10^5$. Left: at $z = 0$, middle: at $z = 0.1$, right: at $z = 0.2$.

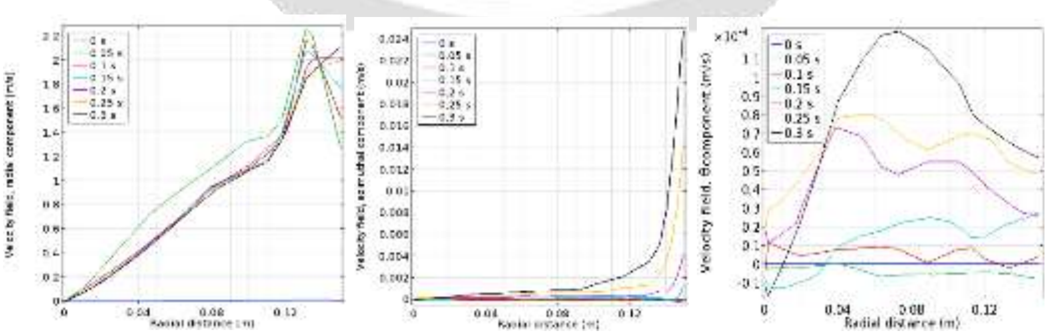

Chart - 18: Azimuthal velocity when $\Gamma = 1.33$ and $\mathrm{Re} = 10^6$. Left: at $z = 0$, middle: at $z = 0.1$, right: at $z = 0.2$.

3.3 Flow in vertical direction

The vertical component of the velocity is growing with time excepted at the bottom where its magnitude remains in the same scale through time (**Chart - *19*** to **Chart - *27*** left). u_z is also increasing with increasing Reynolds number, but it has the same scale when Γ is varying. The vertical velocity is weak at $z=0$ and $z=H$ (**Chart - *19*** to **Chart - *27*** left and right) compared to its value at $z=H/2$ (**Chart - *19*** to **Chart - *27*** middle). At $z=H/2$ and $z=H$, u_z is negative near the center of the container and positive near the sidewall (**Chart - *19*** to **Chart - *27*** middle and right). The flow is then moving upward near the sidewall and downward in the center.

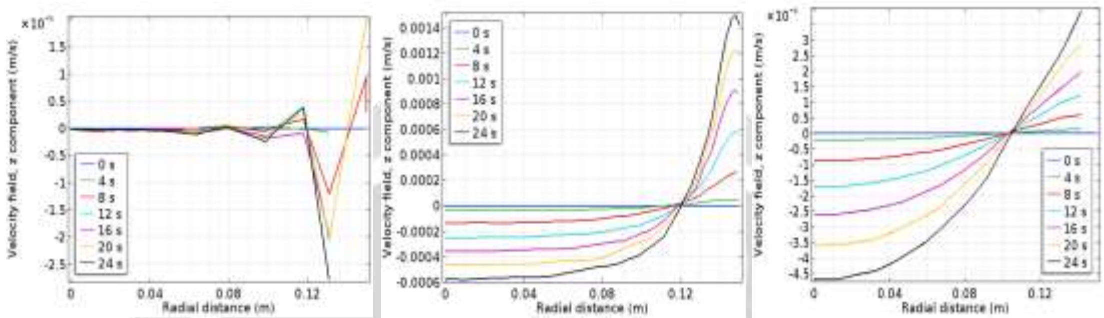

Chart - 19: Vertical velocity when $\Gamma = 0.66$ and $\mathrm{Re} = 10^4$. Left: at $z=0$, middle: at $z=0.05$, right: at $z=0.1$.

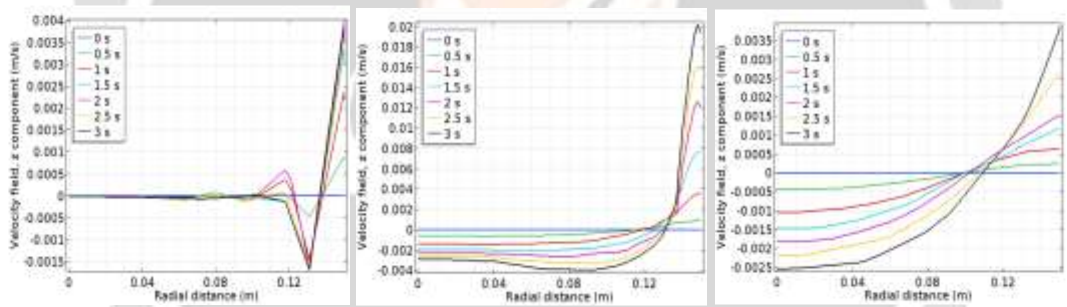

Chart - 20: Vertical velocity when $\Gamma = 0.66$ and $\mathrm{Re} = 10^5$. Left: at $z=0$, middle: at $z=0.05$, right: at $z=0.1$.

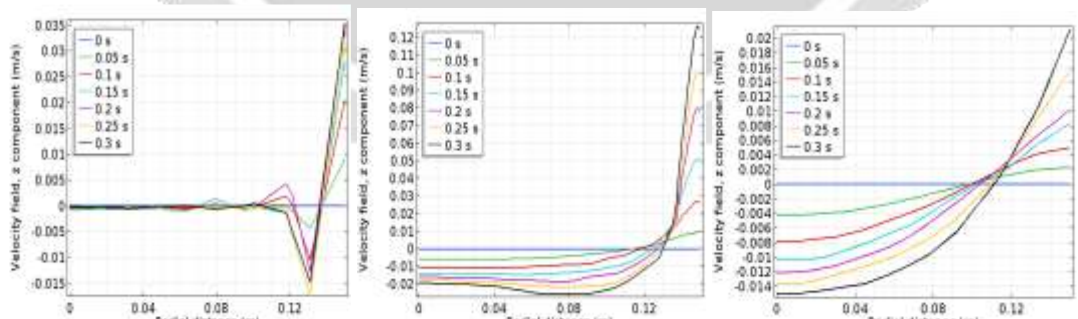

Chart - 21: Vertical velocity when $\Gamma = 0.66$ and $\mathrm{Re} = 10^6$. Left: at $z=0$, middle: at $z=0.05$, right: at $z=0.1$.

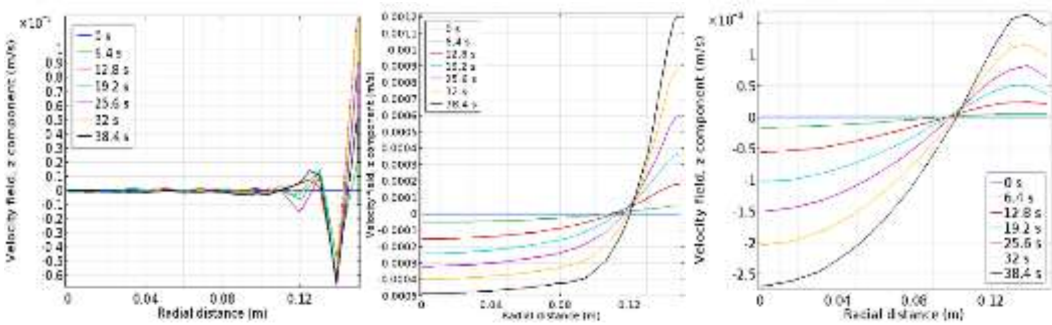

Chart - 22: Vertical velocity when $\Gamma = 1$ and $\mathrm{Re} = 10^4$. Left: at $z = 0$, middle: at $z = 0.075$, right: at $z = 0.15$.

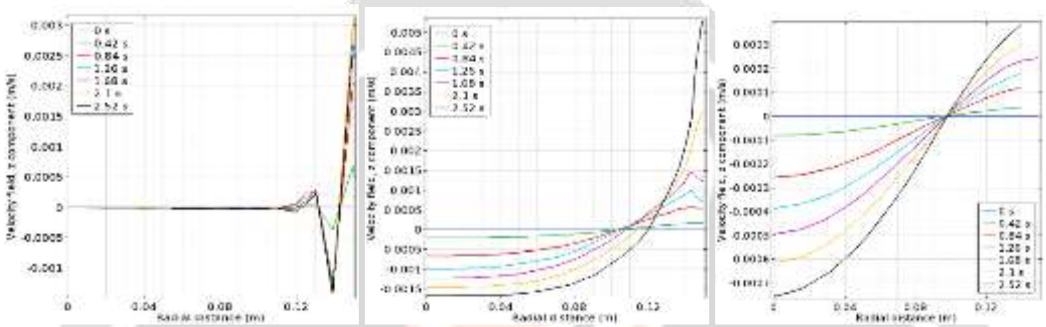

Chart - 23: Vertical velocity when $\Gamma = 1$ and $\mathrm{Re} = 10^5$. Left: at $z = 0$, middle: at $z = 0.075$, right: at $z = 0.15$.

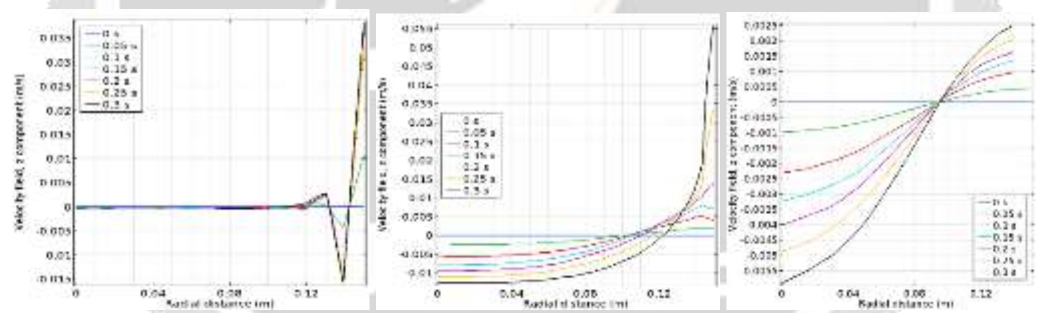

Chart - 24: Vertical velocity when $\Gamma = 1$ and $\mathrm{Re} = 10^6$. Left: at $z = 0$, middle: at $z = 0.075$, right: at $z = 0.15$.

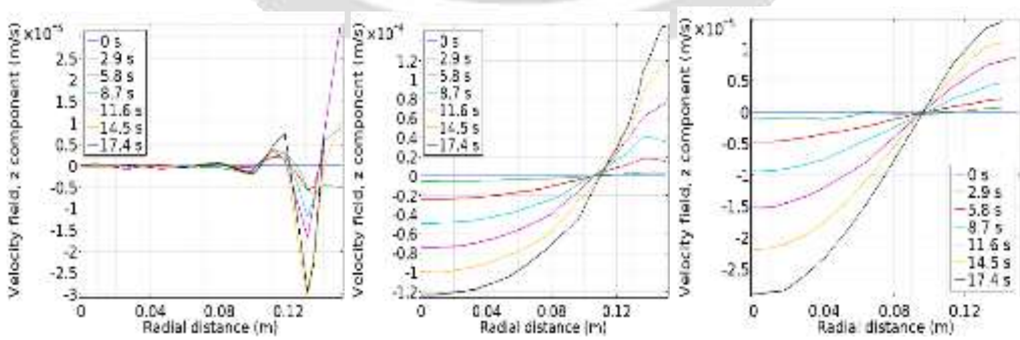

Chart - 25: Vertical velocity when $\Gamma = 1.33$ and $\mathrm{Re} = 10^4$. Left: at $z = 0$, middle: at $z = 0.1$, right: at $z = 0.2$.

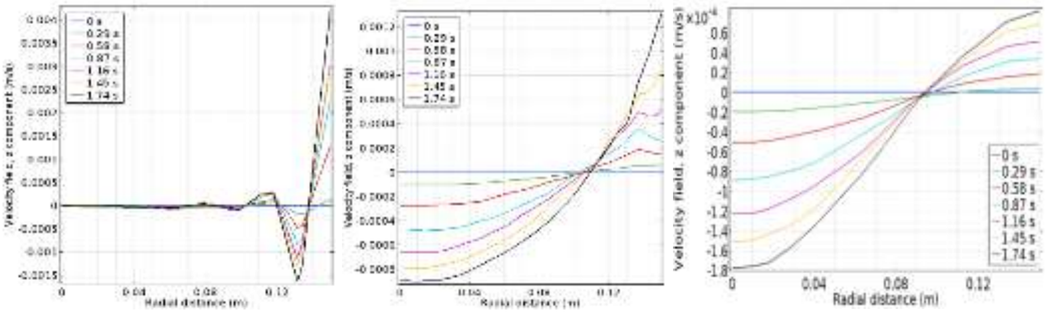

Chart - 26: Vertical velocity when $\Gamma = 1.33$ and $\mathrm{Re} = 10^5$. Left: at $z = 0$, middle: at $z = 0.1$, right: at $z = 0.2$.

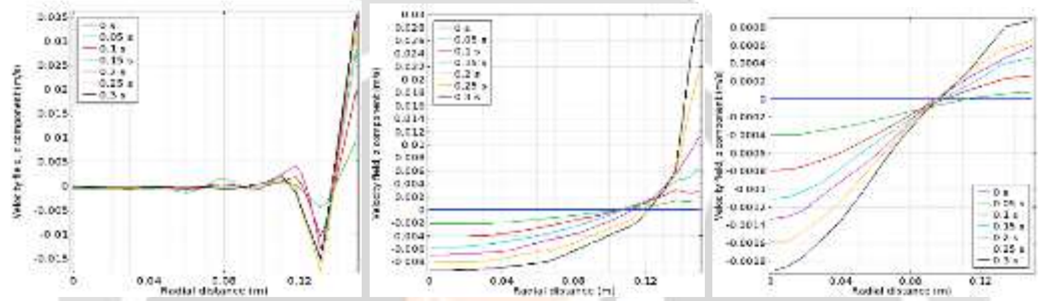

Chart - 27: Vertical velocity when $\Gamma = 1.33$ and $\mathrm{Re} = 10^6$. Left: at $z = 0$, middle: at $z = 0.1$, right: at $z = 0.2$.

4. CONCLUSIONS

This work concerns the investigation of the structure of a fluid flow over a rotating disk with free surface. Flow direction, velocity magnitude variation through time and through space have been studied by varying two parameters: the Reynolds number Re and the aspect ratio Γ of the cylinder. The values of Re used are 10^4, 10^5 and 10^6, and 0.66, 1 and 1.33 for the aspect ratio.

Velocity magnitude increases with time and with increasing Re. The variation towards varying Γ depends on the velocity component. Radial and azimuthal components decrease when Γ grows, while the vertical component keeps the same scale. As regards the fluid motion, the flow is centrifugal at the rotating disk, then the fluid is upward near the fixed sidewall, centripetal at $z = H/2$ and $z = H$, and finally downward at the center of the tank. The direction of rotation is the same as the bottom plate.

The same characteristics as in experimental cases are found concerning the direction of the motion. Future studies will be devoted to the investigation of other characteristics of the flow and the polygonal patterns at the free surface.

5. REFERENCES

[1]. Mougel, Jérôme and Fabre, David and Lacaze, Laurent and Bohr, Tomas. On the instabilities of a potential vortex with a free surface. (2017) Journal of Fluid Mechanics, vol. 824. pp. 230-264. ISSN 0022-1120. DOI: 10.1017/jfm.2017.341.

[2]. Laust Tophoj, Jerome Mougel, Tomas Bohr, David Fabre. Rotating Polygon Instability of a Swirling Free Surface Flow. Physical Review Letters, American Physical Society, 2013, vol. 110, pp. 1-5. <10.1103/PhysRevLett.110.194502>. <hal-00914775>.

[3]. Yang, Wen, Delbende, Ivan, Fraigneau, Yann et Witowski, Laurent Martin, Axisymmetric rotating flow with free surface in a cylindrical tank, J. Fluid Mech., page 1 of 19. © Cambridge University Press 2018. DOI:10.1017/jfm.2018.929.

[4]. Mougel, Jérôme and Fabre, David and Lacaze, Laurent Waves and instabilities in rotating free surface flows. (2014) Mechanics and Industry, vol. 15 (n° 2). pp. 107-112. ISSN 2257-7750. DOI: 10.1051/meca/2014007.

[5]. Bergmann, R. and Tophoj, Laust and Homan, T. A. M. and Hersen, Pascal and Andersen, A. and Bohr, Tomas J., Polygon formation and surface flow on a rotating fluid surface, Fluid Mech., page 1 of 17, Cambridge University Press 2011. DOI:10.1017/jfm.2011.152.
[6]. Jansson, T. R. N., Haspang, M. P., Jensen, K. H., Hersen, P., & Bohr, T. (2006). Polygons on a rotating fluid surface. Physical Review Letters, 96(17), 174502. DOI : 10.1103/PhysRevLett.96.174502.
[7]. Mougel, Jérôme and Fabre, David and Lacaze, Laurent Waves and instabilities in rotating free surface flows. (2014) Mechanics and Industry, vol. 15 n° 2). pp. 107-112. ISSN 2257-7750. DOI : 10.1051/meca/2014007.
[8]. Iima, M. and Tasaka, Y., Dynamics of flow structures and surface shapes in the surface switching of rotating fluid, Journal of fluid mechanics, 789 : 402-424, 2016-02.
[9]. Sébastien Poncet. Polygons on a rotating thin-water layer : a combined experimental and numerical approach. Topical Problems of Fluid Mechanics, Feb 2014, Prague, Czech Republic. 2014. <hal-01098570>
[10]. Giancarlo Alfonsi, Reynolds-Averaged Navier–Stokes Equations for Turbulence Modeling, article in Applied Mechanics Reviews · July 2009. DOI : 10.1115/1.3124648.
[11]. Osher, S. and Sethian, J.A.,Fronts Propagating with Curvature De-pendent Speed: Algorithms Based on Hamilton-Jacobi Formulations, J.Comput. Phys. 79, 12-49 (1988).